Metallacycles Capabilities in Host–Guest Chemistry

Miguel Ponce-Vargas*[a]

Host–guest chemistry encompasses the study of highly structured molecular complexes composed of at least two entities associated by noncovalent interactions, one possessing convergent binding sites, the host, and another possessing divergent binding sites, the guest. Among other species, the host can be a crown ether, calixarene, or metallacycle, whereas the guest can be virtually any small-to-medium size species. The host molecule recognizes those guest entities that contain the array of binding sites and steric features that complement it, with coupling interactions varying from ion–multipole to dispersion forces.

The hollow structure of metallacycles allows them to act as hosts for multiple species. Examples include $[TiO(O_2CC_6F_5)_2]$, capable of interacting simultaneously with two toluene molecules; [15-$MC_{Cu(II)N(picha)}$-5] (picha = picoline hydroxamic acid), which can accommodate lanthanide ions in its cavity; and the rhenium-based systems $[\{(CO)_3Re(\mu\text{-}L)Re\text{-}(CO)_3\}_2(\mu\text{-}4,4'\text{-bipy})_2]$ (L = 5,8-dyhidroxy-1,4-naphtoquinone), which selectively recognizes benzene molecules. The metallacycle host interacts with the guest species via oxygen or nitrogen atoms located within the supporting ligands, while only to a minor extent, the metal centers play this role, giving rise to a more interesting scenario where the nature of the host–guest interactions is related to these uncommon binding sites. Therefore, a study of the electronic structures of metallacycle hosts, focused mainly on the metal centers, will give us a deeper knowledge of the host–guest interactions in inorganic systems. The host–guest interactions can be explored by three methods: 1) energy decomposition analysis (EDA) according to the Morokuma–Ziegler scheme, a method that provides a bridge between the physical laws of quantum mechanics and heuristic models of chemistry; 2) multipole moment tensors, which allow us to measure the departure from spherical symmetry experienced by the metal centers with guest inclusion; and 3) noncovalent index (NCI) analysis, which enables the real-space visualization of the region where noncovalent interactions occur, based on electron density properties.

Two representative series of metallacycle systems have been selected for this research, the halide-centered hexanuclear copper(II) pyrazolate complexes [trans-$Cu_6(3,5\text{-}(CF_3)_2pz)_6(OH)_6X]^-$ (X=F, Cl, Br, I), synthesized by Mohamed and co-workers, and the di-halide cyclic pentameric perfluoroisopropylidene-mercury complexes $[(HgC(CF_3)_2)_52X]^{2-}$ (X=Cl, Br, I), synthesized by Antipin and co-workers, both with metal centers acting as binding sites and halide ions as guest species (Scheme 1).

[a] Dr. M. Ponce-Vargas
Institut des Sciences Chimiques de Rennes UMR 6226
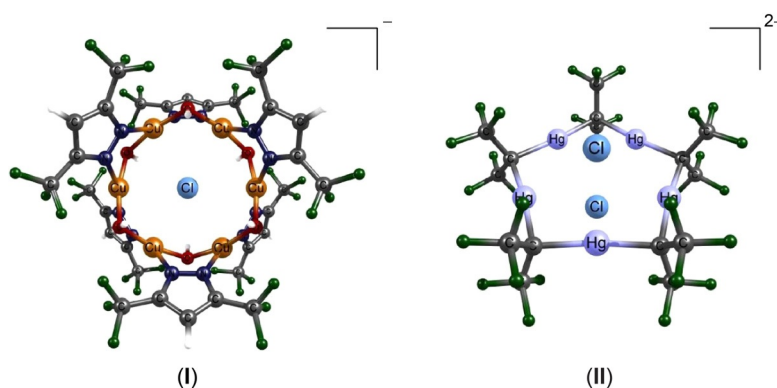Université de Rennes 1, Campus de Beaulieu
35042 Rennes (France)
E-mail: miguel-armando.ponce-vargas@univ-rennes1.fr

Scheme 1. Metallacycle complexes that were the subject of this study: [*trans*-Cu$_6$(3,5-(CF$_3$)$_2$pz)$_6$(OH)$_6$Cl]$^-$ (**I**) and [(HgC(CF$_3$)$_2$)$_5$2Cl]$^{2-}$ (**II**).

Relativistic density functional theory (DFT) calculations have been conducted using the ADF 2012.02 code via the scalar ZORA Hamiltonian, with a triple-ξ Slater basis set plus a polarization function (STO-TZP), and the *meta*-generalized gradient approximation of Tao, Perdew, Staroverov, and Scuseria (TPSS). Geometry optimizations were carried out via the analytical energy gradient method implemented by Verluis and Ziegler, with the inclusion of the dispersion Grimme correction. The local multipole moments calculations were conducted according to the scheme proposed by Swart and co-workers, whereas the graphical representation of the quadrupole tensors is based on the Autschbach methodology. Finally, the NCI analysis was carried out with the NCIPLOT-3.0 program developed by Weitao Yang and co-workers.

In the halide-centered hexanuclear copper(II) pyrazolate complexes [*trans*-Cu$_6$(3,5-(CF$_3$)$_2$pz)$_6$(OH)$_6$X]$^-$ (X=F, Cl, Br, I), denoted as **1**–X, the EDA reveals that the fluorine complex (**1**–F) is the most favorable structure (−79.43 kcal mol^{-1} of total interaction energy ΔE_{int}), followed by the chloride (−73.00 kcal mol^{-1}), bromide (−69.81 kcal mol^{-1}) and iodide (−60.12 kcal mol^{-1}) systems, suggesting that the copper metallacycle exhibit a preference for hard bases. These results are determined in a great extent by the magnitude of the destabilizing Pauli term (ΔE_{Pauli}), which decreases the total interaction energy as the guest size increases.

The stabilization energy given by the dispersion term (ΔE_{disp}) increases within the series, where the iodide host–guest system (**1**–I) presents the largest dispersion energy term (−11.04 kcal mol^{-1}), followed by the bromide (−9.25 kcal mol^{-1}), chloride (−7.54 kcal mol^{-1}) and fluoride (−4.30 kcal mol^{-1}) complexes (Table 1)

The electrostatic contribution to total interaction energy (ΔE_{elec}) represents about 70 % of stabilizing energy, playing a more important role than the orbital interaction ($\sim$25 %), thus denoting the mainly electrostatic character of the host–guest coupling. This behavior can be attributed to the relevance of the ion–multipole interactions (ion–dipole, ion–quadrupole, quadrupole–dipole and quadrupole–quadrupole) between the binding sites of the host, namely the Cu^{II} centers, and the guest, resulting in the stabilization of the host–guest pair.

The multipole moment analysis shows that local dipole moment at the Cu^{II} site increases from 0.041 Debye (D) in **1** to 0.094 D in **1**–F, 0.174 D in **1**–Cl, 0.207 D in **1**–Br, and 0.343 D **1**–I. In all cases, the dipole moment vector points toward the guest, denoting that ion–dipole interaction is located at the Cu$_6$ plane, as is represented in Figure 1. These results suggest the versatility of the Cu^{II} center, which can modulate their dipole moment according to the incoming guest.

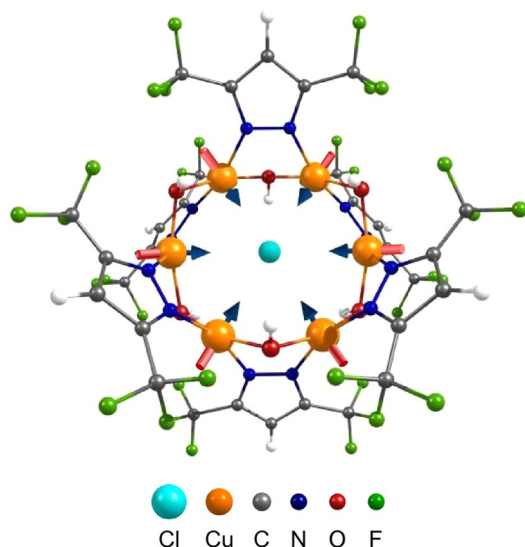| **Table 1.** Energy decomposition (EDA) values (kcal mol^{-1}) of **1**–X systems.				
	1–F	**1**–Cl	**1**–Br	**1**–I
ΔE_{orb}	−34.15	−32.60	−33.28	−37.73
ΔE_{elec}	−57.34	−91.09	−123.24	−165.45
ΔE_{disp}	−4.30	−7.54	−9.25	−11.04
ΔE_{Pauli}	16.36	58.23	95.96	154.10
ΔE_{int}	−79.43	−73.00	−69.81	−60.12

Figure 1. Graphical representation of copper dipole moments in **1**–Cl, where the blue arrowhead denotes the negative region of the local dipole.

With the aim to evaluate higher order Coulombic terms, such as quadrupole–dipole and quadrupole–quadrupole, we include the analysis of the hypothetical noble gas pyrazolate complexes (**1**–Ng). Noble gases are isoelectronic with the corresponding halides, allowing us to evaluate uncharged species directly related to **1**–X, with a decreased electrostatic contribution of the ion–multipole term.

In the EDA of the **1**–Ng series, the electrostatic contribution decreases in a noteworthy manner to values in the range of -2.89 kcal mol^{-1} to -38.07 kcal mol^{-1}, in contrast to the halide case (-57.34 kcal mol^{-1} to -165.45 kcal mol^{-1}), which could be attributed to the cancellation of ion–multipole interactions leading to only quadrupole–dipole and quadrupole–quadrupole forces. The dispersion interaction energies in the **1**–Ng series remain almost unaltered; however, their relative contribution represents now about 27 % of the stabilizing energy. The contribution of the ion–multipole terms to the electrostatic term in the halide series (**1**–X) is calculated as $(1 - {}^{Ng}\Delta E_{elec}/{}^{X}\Delta E_{elec})\cdot 100$, where ${}^{Ng}\Delta E_{elec}$ and ${}^{X}\Delta E_{elec}$ denote the electrostatic term of the noble gases and the halide ions, respectively. Results reveal that ion–multipole contribution to the electrostatic term ranges from 95.0 % to 77.0 % going from **1**–F to **1**–I. Consequently, the contribution of higher-order interactions such as quadrupole–dipole and quadrupole–quadrupole forces, increases from 5.0 % to 23.0 % according to the inclusion of hard, intermediate and soft Lewis bases given by F$^-$, Cl$^-$, Br$^-$, I$^-$.

In order to evaluate the charge redistribution occurring as a consequence of the host–guest coupling, natural population analyses (NPA) for **1** and the **1**–X series were carried out by using the stand-alone NBO5 suite. The inclusion of the halide guest gives rise to an electron-density transfer, leading to an average $-0.86\,|e|$ charge at the halide ions, which varies in line with the ΔE_{orb} term. The guest incorporation also causes a variation in the copper charges toward more positive values, suggesting a displacement of the electronic density from the metal centers to the pyrazolate groups. Then, both the charge of the incoming guest and that leaving the copper centers, are mainly distributed over the pyrazolate derivative as is reflected by a charge variation of about $0.18\,|e|$ associated to these groups.

Additionally, we studied the role of the highly electronegative fluorine atoms into the charge-transfer process, through an NPA for the hypothetical system trans-Cu$_6\{\mu$-3,5-(CH$_3$)$_2$pz$\}_6(\mu$-OH)$_6$ (**2**) and its corresponding complexes [trans-Cu$_6\{\mu$-3,5-(CH$_3$)$_2$pz$\}_6(\mu$-OH)$_6$X]$^-$ (X=F, Cl, Br, I) (**2**–X), where the trifluoromethyl substituents are replaced by methyl groups. We can observe a decrease in the charge transfer from the guest species to the metallacycle host evidenced by the $-0.90\,|e|$ average charge in the halide ions. Also we noticed how the pyrazolate derivatives experience a slight charge variation of around $0.05\,|e|$ with the guest entry. This NPA reveals the importance of the trifluoromethyl groups in promoting the charge-transfer process occurring during the host–guest coupling.

To obtain a clear representation of the distortion from spherical symmetry experienced by the electronic density at the guest and host binding sites, we evaluated the corresponding quadrupole moment tensors, including their graphical representation as an isosurface, similarly to other second-rank tensor magnitudes. A set of principal axes can always be found such as the off-diagonal elements vanish leading to the principal axis representation, where the tensor is depicted in its own framework. The graphical representation of the quadrupole tensors is given in Figure 2.

In our particular case with **1**–X belonging to the D_{3d} symmetry point group, the central guest describes a relationship given by $\Theta_{11} = \Theta_{22} \neq \Theta_{33}$, where the axial component (Θ_{33}) presents negative values and the perpendicular components Θ_{11} and Θ_{22} positive ones. This means that the guest quadrupole moment is distorted axially, being the electronic charge removed from the C$_6$ plane and con-
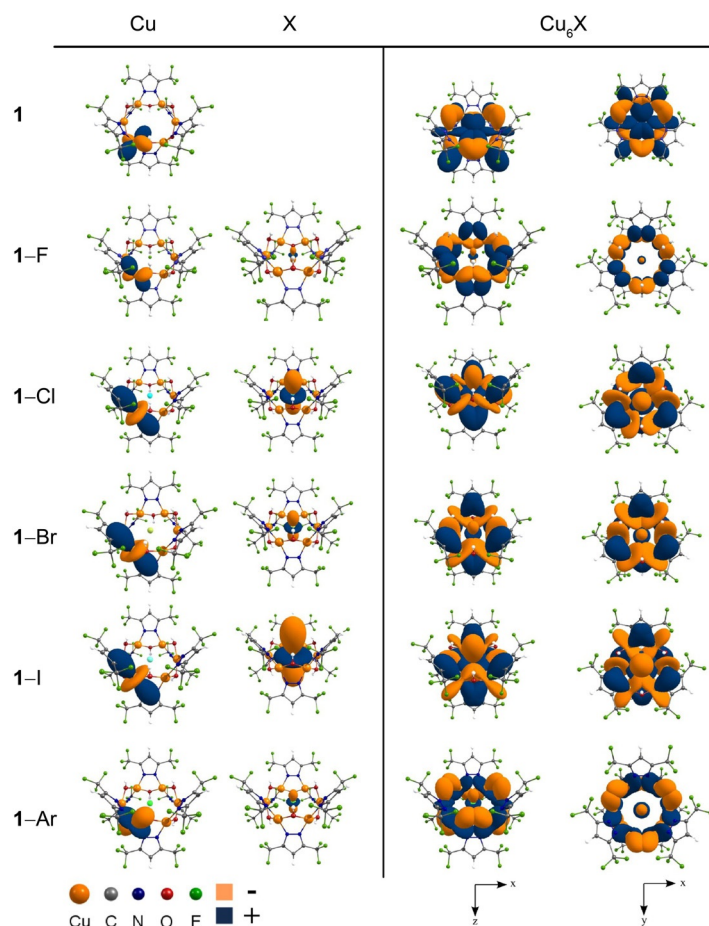
Figure 2. Graphical representation of the electric quadrupole tensors of the studied systems.

centrated along the main axis. This distortion of the electronic density could be attributed to the dipole–quadrupole host–guest interactions occurring in such plane, in addition to the ion–dipole interaction.

In order to quantify the quadrupole moment distortion from spherical symmetry, we introduce the quadrupole anisotropic component (Θ_{aniso}) in analogy to the Haeberlen convention. The more polarizable iodide guest exhibits the largest Θ_{aniso} value, which accounts for the higher ΔE_{elec} term couple inside the series.

The six Cu^{II} centers, considered as borderline Lewis acids according to the Pearson hard and soft acids and bases (HSAB) principle, experience different distributions of the electron density in each complex, varying its quadrupole moment according to the hardness of the involved guest, reaching its maximum value in **1**–I. In Figure 2, it can be observed the variation of the local quadrupole of a representative Cu^{II} center, where for **1**, the local quadrupole moment components are mainly distributed over two principal axes, the first one pointing toward the metallacycle center ($^{Cu}\Theta_{11}$), and the second one defined by the Cu–O bond ($^{Cu}\Theta_{33}$).

In the host–guest complexes, the local quadrupole exhibits a different shape driven by the electron-rich region now located between the Cu–O and Cu⋯X regions. Going from **1**–F to **1**–I, the $^{Cu}\Theta_{33}$ component is located in a large extent toward the axis determined by the Cu⋯X interaction, resulting in a negatively charged region at the Cu$_6$ plane, whereas the electro-positive component ($^{Cu}\Theta_{11}$) is oriented along the Cu–N bond, generating positively charged regions above and below the Cu$_6$ ring. We suggest that these electron-deficient regions are those that mainly interact with the negative axial distribution of the guest, leading to quadrupole–quadrupole forces. Interestingly, the $^{Cu}\Theta_{33}$ guest axial component reaches its more negative value in **1**–I, where a more effective match occurs with the metallacycle electron-deficient regions defined by the copper quadrupole positive lobes. Thus, this methodology gives a clear description of quadrupole–quadrupole host–guest forces, which are mainly lo-
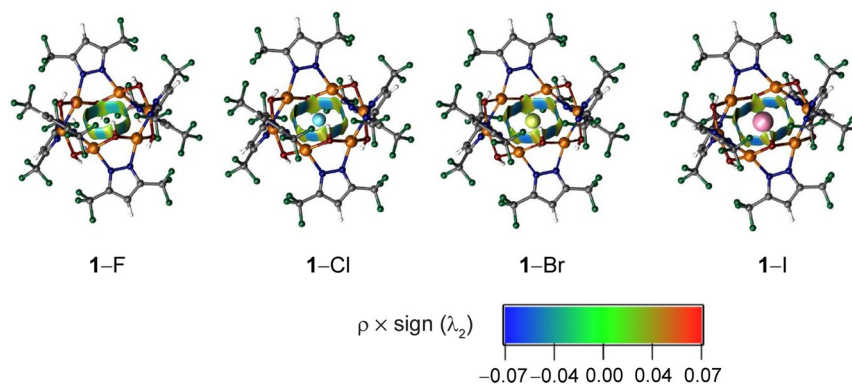
Figure 3. Noncovalent index (NCI) analysis for the halide complexes **1**–X (X = F, Cl, Br, I).

cated above and below the Cu_6 plane, in contrast to the ion–dipole and quadrupole–dipole interactions, located in the Cu_6 plane.

The observed variation of the quadrupole moment of the host Cu^{II} centers reveals that metallacycles acting as hosts can offer clear advantages in comparison to their organic counterparts, prompted by the versatility of their metal centers capable to adjust their electron densities according to the incoming guest, leading to different ranges of electron-density anisotropies (Θ_{aniso}), associated to electron density fluctuations, and hence, to noncovalent interactions.

The NCI analysis for the **1**–X series is presented in Figure 3, where for all systems, the region involving noncovalent interactions is located between the Cu_6 ring and the central guest. This region denotes stabilizing forces between the copper centers and the guest species, supporting our statement that metal centers act as binding sites.

The same procedure followed with **1**–X is applied to the halide cyclic pentameric perfluoroisopropylidenemercury complexes $[(HgC(CF_3)_2)_5 2X]^{2-}$ (X=Cl, Br, I), where two guests interact simultaneously with five mercury(II) centers. In this case, the preference for the chloride guests is evidenced by a total interaction energy (ΔE_{int}) of $-186.16\ kcal\,mol^{-1}$. The EDA also suggests the electrostatic character of the host–guest pair, which is ruled by the ion–multipole term by about 97%, favoring the inclusion of the hardest ion. Interestingly, in this series, higher-order Coulombic terms do not arise in a great extent even in the iodide system. It seems that mercury linear local geometry given by the Hg–C bonds, and the D_{5h} molecular symmetry determine the shape of the local quadrupole moments at the binding sites leading to an in-plane distribution, preventing the arise of a significant quadrupole component perpendicular to the Hg_5 plane that can contribute to higher-order electrostatic terms, related to the preference for the iodide guest. Additionally, by using the NPA, the importance of trifluoromethyl groups in promoting the electron-charge transfer is evidenced once again.

As concluding remarks, we can mention that the methodologies here employed allowed us to determine the mainly electrostatic character of host–guest interactions in metallacycle-based complexes and to weigh the role of certain Coulombic terms, leading to a clear rationalization of the host–guest coupling. Additionally, our methodology involving the plot of the quadrupole moment tensors provides a clear representation of the higher-order electrostatic interactions within the studied systems, such as dipole–quadrupole and quadrupole–quadrupole forces.

Publications arising from this work:
- M. Ponce-Vargas, A. Muñoz-Castro, *J. Phys. Chem. C* **2014**, *118*, 28244–28251.
- M. Ponce-Vargas, A. Muñoz-Castro, *Phys. Chem. Chem. Phys.* **2014**, *16*, 13103–13111.
- M. Ponce-Vargas, A. Muñoz-Castro, *Phys. Chem. Chem. Phys.* **2015**, *17*, 18677–18683.